Journal Pre-proof

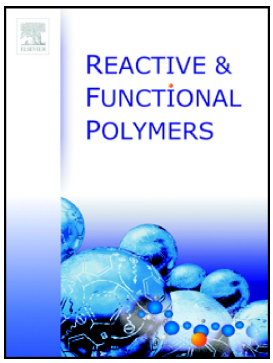

Zn(II) detection in biological samples with a smart sensory polymer

Marta Guembe-García, Saúl Vallejos, Israel Carreira-Barral, Saturnino Ibeas, Félix C. García, Victoria Santaolalla-García, Natalia Moradillo-Renuncio, José M. García

PII: S1381-5148(20)30519-8

DOI: https://doi.org/10.1016/j.reactfunctpolym.2020.104685

Reference: REACT 104685

To appear in: *Reactive and Functional Polymers*

Received date: 6 May 2020

Revised date: 16 June 2020

Accepted date: 27 June 2020

Please cite this article as: M. Guembe-García, S. Vallejos, I. Carreira-Barral, et al., Zn(II) detection in biological samples with a smart sensory polymer, *Reactive and Functional Polymers* (2019), https://doi.org/10.1016/j.reactfunctpolym.2020.104685

Zn(II) detection in biological samples with a smart sensory polymer

Marta Guembe-García,[1] Saúl Vallejos,[1,*] Israel Carreira-Barral,[1] Saturnino Ibeas,[1] Félix C. García,[1] Victoria Santaolalla-García,[2] Natalia Moradillo-Renuncio,[2] José M. García[1,*]

[1] Departamento de Química, Facultad de Ciencias, Universidad de Burgos, Plaza de Misael Bañuelos s/n, 09001 Burgos, Spain. E-mail: jmiguel@ubu.es (J.M.G.), svallejos@ubu.es (S.V.)
[2] Complejo Asistencial Universitario de Burgos, Burgos, Spain
* Correspondence: svallejos@ubu.es (S.V.); jmiguel@ubu.es (J.M.G.)

Abstract: We have developed a new sensory material for the rapid and inexpensive determination of Zn(II), and we have carried out a proof of concept for the determination of Zn(II) in biological samples. The interaction with Zn(II) generates an OFF-ON fluorescence process on the material, which can be recorded both with a fluorimeter and with a smartphone by analyzing the RGB components of the taken photographs. This sensory material is prepared with 99.75% of commercially available monomers and contains 0.25% of a sensory monomer based on a quinoline structure. The sensory motifs are chemically anchored to the polymeric structure, and, accordingly, no migration of organic substances from the material occurs during the sensing process. Our method has been tested with freshly prepared Zn(II) aqueous solutions, but also with biological samples from exudates of chronic wounds. The proposed methodology provides limits of detection (LOD) of 13 and 2.7 ppb when employing a water-soluble polymer (WsP) and a hydrophilic polymeric film (HF), respectively, using emission spectroscopy. The measurements have been contrasted with ICP-MS as the reference method, obtaining reliable data. This study is the starting point towards a larger investigation with patients, which will address the challenge of establishing a direct relationship between the concentration of zinc(II), other cations and also of amino acids, with the protease activity and, finally, with the state/evolution of chronic wounds. In this context, the proposed sensory material and others we are now working with will act as a simple and cheap method for this purpose.
Keywords: smart materials; sensory polymers; zinc(II) detection; biological samples; chronic wounds.

1. Introduction

Zn(II) is an essential element for human body. It is found in secretions such as urine, sweat, semen, and hair, but it is mostly located in muscles and bones [1]. The concentration of Zn(II) can be especially high in some organs, such as liver or skin, where up to 5% of all the Zn(II) present in the human body can be found. Regarding cells, Zn(II) can reach pico- to nanomolar concentrations inside, and micromolar concentrations in the extracellular space [2].

Also, Zn(II) is part of more than 300 enzymes with different functions, in which it is present as a structural, catalytic and/or regulatory component [3,4]. Given this multifunctionality of Zn(II), the deficiency of this ion has a great impact on the organism, and it is related to gastrointestinal disorders,[5] kidney and liver diseases [6], dermatitis [7], hypogonadism [8], or impartial wound healing [9,10]. In fact, the relationship between Zn(II) deficiency and impaired wound healing has been a research topic in recent years [11,12].

Other authors have studied the relationship between Zn(II) and prostate cancer, developing specific markers of Zn(II) to monitor the disease [13]. To assess the Zn(II) status in the body, serum, plasma, and erythrocyte levels are used as biomarkers [14–19]. In day to day, hospital laboratories analyze serum zinc(II) by UV-Vis spectrophotometry, especially to adjust the Zn(II) percentage in parenteral nutrition, but this methodology requires expensive equipment and skilled people.

Smart sensory polymers are a really hot topic [20–24], and have provided good results with easy procedures [25], so we propose a rapid, inexpensive and easy-to-use sensory material, which generates a visual fluorescent response measurable with a simple smartphone. Our material will provide rapid information about the Zn(II) concentration of the biological sample; corrective personalized treatments could be applied by the medical staff. The main objective of this study is to prepare a polymeric sensory material for the easy and rapid detection of Zn(II), taking into consideration that not all Zn(II) is accessible; for example, when coordinated as a structural or catalytic component in different enzymes. Thus, we have designed a sensory material with quinoline-based receptors for the recognition of this metal ion, the complex formation being highly favorable from the thermodynamic point of view [26–29]. Our quinoline derivative is based on the 'Zinquin' (CAS number: 151606-29-0) structure, a commercially available reagent [30], which behaves as a membrane-permeable fluorophore and is commonly used to detect Zn(II) in cells [31] and to control the change in intracellular Zn(II) concentrations in thymocytes and hepatocytes [32].

Our sensory material has been tested with freshly prepared Zn(II) aqueous solutions and, most importantly, with real samples obtained from exudates of chronic wounds, following procedures established by the Vascular Surgery Unit at Burgos University Hospital (HUBU). This is the first of a set of studies devoted to prepare a sensory material which will act as a simple and cheap method to analyze relationships between the concentration of zinc(II), other cations and amino acids, and the protease activity of chronic wounds as well as the state/evolution of these wounds.

2. Experimental

2.1. Materials

Materials and solvents are commercially available and were used as received unless otherwise indicated. The following materials and solvents were employed: *trans*-crotonaldehyde (≥99%, Sigma-Aldrich), 3,4-dinitrophenol (98%, Acros Organics), palladium on carbon (10%, Sigma-Aldrich), ethanol absolute (100%, VWR), methanol (100%, VWR), dichloromethane (100%, VWR), hexane (95%, VWR), ethyl acetate (99.9%, VWR), thionyl chloride (99%, VWR), sodium 4-vinylbenzenesulfonate (≥90%, Sigma-Aldrich), dimethylformamide (99%, VWR), diethyl ether (99.7%, VWR), sodium sulfate (≥99%, VWR), pyridine (99.5%, Merck), 2,2'-azobis(2-methylpropionitrile) (AIBN) (98%, Aldrich), 1-vinyl-2-pyrrolidone (**VP**) (99%, Acros Organics), methylmethacrylate (**MMA**) (99%, Merck), pH 4.66 buffer (VWR), zinc(II) nitrate hexahydrate (98%, Sigma-Aldrich), quinine sulfate (99%, Sigma-Aldrich), cesium nitrate (≥99%, Fluka), manganese(II) nitrate hexahydrate (98+%, Alfa Aesar), tetrachloroauric(III) acid trihydrate (99.9+%, Sigma-Aldrich), potassium dichromate (≥99.5%, Sigma-Aldrich), barium chloride dihydrate (99%, Labkem), cobalt(II) nitrate hexahydrate (≥99%, Labkem), ammonium nitrate (≥98%, Sigma-Aldrich), calcium nitrate tetrahydrate (≥99%, Sigma-Aldrich), chromium(III) nitrate nonahydrate (98.5%, Alfa Aesar), mercury(II) nitrate (98%, Alfa Aesar), rubidium nitrate (99.95%, Sigma-Aldrich), dysprosium(III) nitrate (99.9%, Alfa Aesar), lithium chloride (≥99%, Sigma-Aldrich), cadmium nitrate tetrahydrate (98.5%, Alfa Aesar), iron(III) nitrate nonahydrate (VWR-Prolabo), cerium(III) chloride tetrahydrate (≥99.99%, Sigma-Aldrich), zirconium(IV) chloride (98%, Alfa Aesar), lanthanum(III) nitrate hexahydrate (99.9%, Alfa Aesar), potassium nitrate (99+%, Sigma-Aldrich), samarium(III) nitrate (99.9%, Alfa Aesar), magnesium nitrate hexahydrate (≥99%, Labkem), aluminum nitrate nonahydrate (≥98.9%, Sigma-Aldrich), silver nitrate (≥99.9%, Sigma-Aldrich), neodymium(III) nitrate (99.9%, Alfa Aesar), lead(II) nitrate (≥99%, Fluka), strontium nitrate (99+%, Sigma-Aldrich), copper(II) nitrate trihydrate (98%, Sigma-Aldrich), nickel(II) nitrate hexahydrate (98.5%, Sigma-Aldrich), sodium nitrate (99%, LabKem), tin(II) chloride (98%, Sigma-Aldrich) and zinc(II) chloride (≥98%, Sigma-Aldrich).

Real biological samples (exudates) were removed from chronic wounds in patients admitted at the Vascular Surgery Unit in HUBU. According to the status of the patient and considering the needs of each particular wound, a swab was carefully and exhaustively scraped all over the clean loss of substance, under strict aseptic and antiseptic conditions.

2.2. Measurements and instrumentation

The color of each pixel in the RGB color model is expressed indicating how much of the three variables red (R), green (G) and blue (B) define it. The R, G and B triplet defining a digital color in the model can vary from zero to a maximum, typically integers from 0 to 255 in digital cameras of smartphones and computers. In this work we analyze the color of the sensory polymers was using this model, thus considering the digital red (R), green (G) and blue (B) color parameters (RGB) of the material (from now on the RGB method). Digital pictures were taken to the sensory discs (12 mm diameter; this is the inside distance from one corner to the opposite one –diagonal– of a standard 1 x 1 cm fluorescence cuvette) with a Huawei Mate 20 X smartphone after their immersion in aqueous media with different Zn(II) concentrations. To obtain a good reproducibility of the results and to avoid external influences in the photographs, these were taken in a dark room. The digital photographs were analyzed with a generic image software to obtain the RGB parameters of the complete surface of the sensory disc. Photographs were taken six-fold for error calculations, for each the RGB parameters were overaged from the pixels of the overall disc within the picture, and then the six triplet defining the color of the disc (R, G and B variables) were again averaged. For this system, the simple study of each component versus the logarithm of Zn(II) molarity shows that the green component varies linearly with Zn(II) concentration. This easy and cheap method allows the quantification of Zn(II) in aqueous media, by only taking a photo, and we have widely used it in previous works [33,34].

Fluorescence spectra were recorded by triplicate using a F-7000 Hitachi Fluorescence spectrophotometer. Measurements with the water-soluble polymer (**WsP**) were carried out in a conventional cuvette, with no special procedures. However, measurements with the hydrophilic polymeric film (**HP**) were conducted by positioning the membrane vertically in the spectrofluorimeter and at 45° regarding the light source and the detector, as we describe in a previous article [35]. The reflection of light on the film surface was prevented from reaching the detector by placing the discs in a position such that the light source would hit the discs on one side; the other side would emit the detected light, with the reflected one going in the opposite direction.

The starting material was thermally and mechanically characterized using thermogravimetric analysis (TGA, 10–15 mg of a sample under synthetic air and nitrogen atmosphere with a TA Instruments Q50 TGA analyzer at 10 °C·min^{-1}), differential scanning calorimetry (DSC, 10–15 mg of a sample under a nitrogen atmosphere with a TA Instruments Q200 DSC analyzer at 20 °C·min^{-1}), and tensile properties analysis (5 × 9.44 × 0.122 mm samples using a Shimadzu EZ Test Compact Table-Top Universal Tester at 1 mm·min^{-1}). The infrared spectra (FT-IR) of the synthesized compounds and prepared sensory films were recorded using a JASCO FT-IR 4200 (4000-400 cm^{-1}) spectrometer.

High-resolution electron-impact mass spectrometry (EI-HRMS) was carried out on a Micromass AutoSpect Waters mass spectrometer (ionization energy: 70 eV; mass resolving power: >10,000). Inductively coupled plasma mass spectrometry (ICP-MS) measurements were recorded on an Agilent 7500 ICP-MS spectrometer. ^{1}H and ^{13}C NMR spectra were recorded with a Varian Inova 400 spectrometer operating at 399.92 and 100.57 MHz, respectively, with deuterated dimethyl sulfoxide as the solvent. The weight percentage of water taken up by the films upon soaking in pure water at 20 °C until reaching equilibrium (water-swelling percentage, WSP) was obtained from the weight of a dry sample film (ω_d) and its water-swelled weight (ω_s) using the following expression: $WSP=100\times[(\omega_s-\omega_d)/\omega_d]$.

Three-dimensional X-ray data were collected on a Bruker D8 VENTURE diffractometer, and the powder X-ray diffraction (PXRD) patterns were obtained using a Bruker D8 Discover (Davinci design) operating at 40 kV, using Cu(Kα) as the radiation source, a scan step size of 0.02º, and a scan step time of 2 s.

Quantum yields (F) were measured in *N*,*N*-dimethylacetamide (DMA) using quinine sulfate in sulfuric acid (0.05 M) as a reference standard [36].

2.3. Sensory monomer synthesis

The sensory monomer derived from 8-aminoquinoline was prepared and characterized according to the experimental procedure described in the electronic supplementary information, **ESI (Section S1)**, and shown schematically in **Figure 1**.

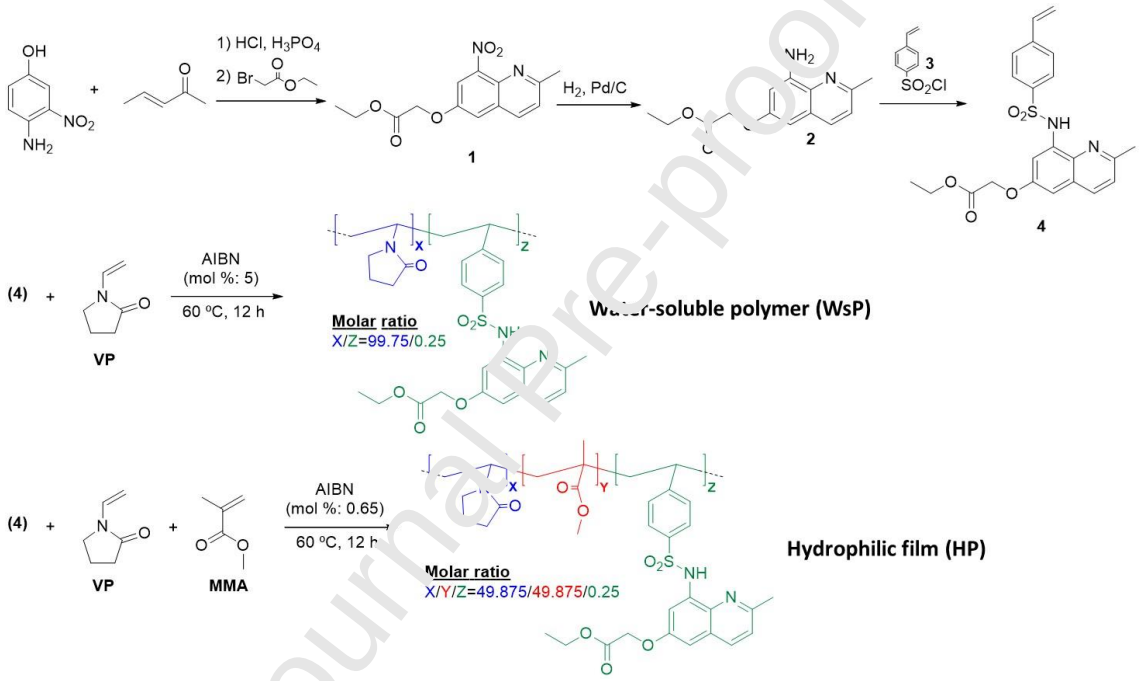

Figure 1. Synthetic route for sensory monomer **4** and its copolymerization with different commercial monomers (**VP** and **MMA**).

2.4. Polymer synthesis

*Water-soluble polymer (**WsP**)*

The linear copolymer (**WsP**) was prepared by radical polymerization of hydrophilic monomer **VP** and sensory monomer **4** in a 99.75/0.25 molar ratio, respectively (**Figure 1**). 0.11 mmol (48 mg) of **4** and 45 mmol (5 g) of **VP** were dissolved in DMF (22 mL) and the solution added to a round-bottom pressure flask. Subsequently, radical thermal initiator AIBN (370 mg, 2.25 mmol, 5% of the total mol amount) was added and the solution sonicated for 10 min; then, it was heated at 60 ºC overnight, under a nitrogen atmosphere and without stirring. The relative high amount of AIBN provides small polymers, or even oligomers, with a molecular mass of around 1000 (measured by ESI-TOF), which favors solubility and does not increase viscosity excessively. After that, the solution was cooled down and added in a dropwise

manner to diethyl ether (300 mL) with vigorous stirring, yielding the desired product as a white precipitate. The water-soluble polymer was purified in a Soxhlet apparatus with diethyl ether as the washing solvent. The final product was dried overnight in a vacuum oven at 60 ^{0}C. Yield: 85%.

*Hydrophilic Film (**HP**)*

The starting material was obtained by radical copolymerization of the different monomers: **VP** as the hydrophilic monomer, **MMA** as the hydrophobic monomer, and **4** as the sensory monomer (**Figure 1**). The bulk radical polymerization was carried out in a silanized glass mold (100 μm thick) in an oxygen-free atmosphere at 60 °C overnight to obtain the hydrophilic film. Regarding the molar ratio of the monomers, this can be adjusted for different purposes. In our case, the fluorimetric response of the material toward Zn(II) was modulated by adjusting the molar feed ratio of monomers to 49.875/49.875/0.25 (**VP**/**MMA**/**4**), using 0.65% mol of AIBN. The relatively small amount of AIBN renders a high molecular mass polymer of around 1x10^{6} (measured by GPC), which gives good mechanical properties to the film.

3. Results and discussion

3.1. Water uptake of the hydrophilic film

The swelling percentage of the hydrophilic film is a critical parameter to obtain a sensory material with good manageability and reasonable response times. This is achieved by reaching the optimum ratio between the hydrophilic co-monomer (**VP**) and the hydrophobic co-monomer (**MMA**), since, if the material swells a lot (above 100%), response times will lower, but manageability will be bad. With swellings below 50%, the workability of the material may be high, but response times will be long. Therefore, given our experience in this area, we propose a material with 60% swelling for this work, which is achieved with a molar percentage of both **VP** and **MMA** of 49.875%. In this case, the molar ratio of the sensory monomer was set at 0.25% to modulate the fluorescent signal according to the fluorimeter.

The three-dimensional hydrophilic film network generates a protective environment for the detection of targets, as we will report, since it reduces the interactions between the sensory monomer receptors and the solvent (water) [37]. This, together with its ability to anchor organic molecules (insoluble in water) in a hydrophilic polymer, favors the Zn(II) detection process within the hydrophilic film.

3.2. Thermal and mechanical characterization

We consider that a material has good manageability when it presents some technical features regarding its thermal and mechanical stability. In this case, the hydrophilic film displays good manageability. TGA analysis shows that T_5 and T_{10} (temperatures at which 5% and 10% weight loss, respectively, was observed) possess values of 345 ^{o}C and 358 ^{o}C, respectively. The material was also characterized by analyzing its glass transition temperature (Tg) by DSC, obtaining a value of 142 ^{o}C. Both TGA and DSC patterns are shown in **ESI (Section S2)**.

Mechanical properties were tested with testing strips cut from the hydrophilic film and dried at 60 ^{o}C for 1 hour. Strips were 0.5 mm wide, 3 cm long, and 0.1 mm thick, and the resulting Young's modulus was 986 MPa. These data confirm the manageability visually observed upon film handling.

3.3. CIE chromaticity coordinates and quantum yield

CIE chromaticity coordinates were calculated from the fluorescence spectra for the determination of the perceived color of **WsP** in the presence of Zn(II) upon irradiation in terms of the corresponding CIE

1931 color matching functions [38]. The results show values for X and Y coordinates of 0.15 and 0.25, respectively, according to the observed blue color. **Figure S4** of **ESI**, **Section S3** displays the CIE chromaticity coordinates (x and y) drawn on the CIE 1931 xy chromaticity diagram. The quantum yield was calculated from a solution of **4** in THF in the presence of one equivalent of Zn(II); quinine sulfate was used as a fluorescence reference in acidic media (0.05 M sulfuric acid) as depicted in previous works [35]. The results show that the Zn(II):**4** complex has a high quantum yield (F = 0.27), a datum similar to that of the reference, quinine sulfate (F = 0.53).

3.4. X-ray diffraction analyses

The solid-state structures of compounds **4** and Zn(II):**4** were determined by using single-crystal X-ray diffraction analyses (see **Figure S5** in **ESI**, **Section S4**, and **Figure 2,** respectively). Crystals of Zn(II):**4** contain the $[Zn(\mathbf{4})Cl_2]^-$ anion, a $(\mathbf{4}\text{-H})^+$ cation and a crystallization water molecule; the presence of both the anionic complex, coming from the deprotonation of the N-H fragment of the sulfonamide group, and the quinolinium cation accounts for the amphoteric nature of the monomer. The metal coordination environment can be described as distorted tetrahedral, with the nitrogen atoms of the sulfonamide and quinoline moieties [N(1) and N(2), respectively] and the two chloride anions [Cl(1) and Cl(2)] occupying the four coordination positions. The average Zn-N and Zn-Cl distances are 2.03 Å and 2.24 Å, respectively, similar to those reported in the literature for other Zn(II) complexes with a tetrahedral environment around the metal centre [39–41]. The distortion of the coordination polyhedron is mainly provoked by the small bite angle of **4** [N(1)-Zn(1)-N(2) 81.2°], which deviates remarkably from the ideal tetrahedral angle (109.5°). This structure is stabilized by slipped π-π stacking interactions involving the quinoline moiety of the protonated monomer and that of the complex (mean centroid···centroid: 3.66 Å), as well as by an array of hydrogen-bonding interactions: among those of moderate strength [42,43], that in which the N-H fragment of the protonated ligand's sulfonamide group and one of the chloride anions are implied [N(4)···Cl(1) 3.17 Å, N(4)-H(4)···Cl(1) 169°] and those involving the water molecule [N(3)···O(11) 2.73 Å, N(3)-H(3)···O(11) 161°, O(11)···O(2) 2.81 Å, O(11)-H(11B)···O(2) 155°]; several weaker contacts are also observed (see **Figure 2**). Overall, this structure shows that, in the solid state, the metal to ligand stoichiometry is 1:1. Crystal data/refinement details and bond distances/angles of **4** and Zn(II):**4** can be found in **Tables S1** and **S2** of **ESI (Section 4)**, respectively.

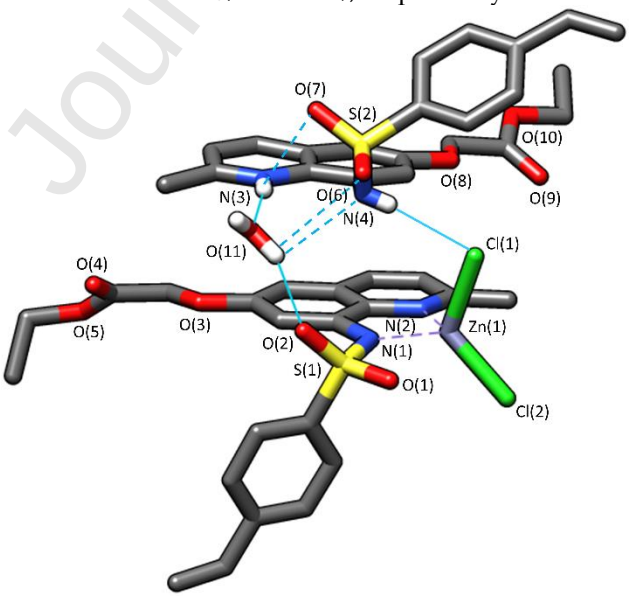

Figure 2. Solid-state X-ray structure of compound Zn(II):**4**. Hydrogen atoms, except those

involved in hydrogen-bonding interactions (the moderate ones are represented by continuous light blue lines and the weaker ones by dotted light blue lines), have been omitted for the sake of simplicity.

3.5. Determination of Zn(II) by fluorimetry

*Using the water-soluble polymer (**WsP**)*

The titration with Zn(II) was carried out by increasing the Zn(II) concentration (from $2.5x10^{-7}$ to $2.7x10^{-3}$ M) in an aqueous solution of **WsP** (2.02 g/L, which corresponded to $4.52x10^{-2}$ milliequivalents of **4** per litre) buffered at pH 4.66 and recording the fluorescence spectra. **Figure 3** depicts the formation of a fluorescence band centered at 460 nm when the sample is irradiated at 370 nm. The Job´s plot diagram (**ESI**, **Section S5**, **Figure S6**) shows that the stoichiometry of the complex formed between the receptors of the polymer (**4**) and the Zn(II) ion is 1:1. The complex formation constant between Zn(II) and **4** amounts to $1.5x10^{5}$, a value that was obtained from the representation of the recorded fluorescence at 460 nm versus the Zn(II) concentration; the fitted curve is shown in **ESI**, **Section S6** and **Figure S8**. The limit of detection (LOD) of this system was 13 ppb. Note that an ICP-MS of **WsP** was necessary for the calculation of the real amount of **4** motifs anchored to the polymer chain (see **ESI**, **Section S7**). Although the polymer was designed with 0.25% mol of **4**, the real concentration obtained from ICP-MS was 0.23%.

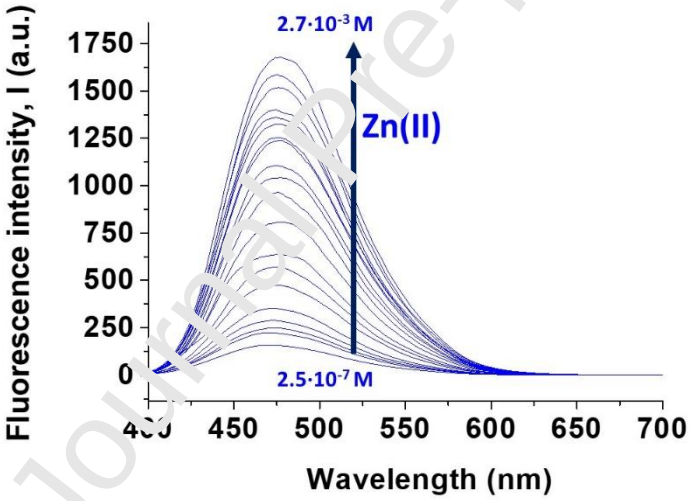

Figure 3. Titration of **WsP** with Zn(II) in an aqueous solution buffered at pH 4.66. The initial concentration of **WsP** in the cuvette was 2.02 g/L, which corresponded to $4.52x10^{-2}$ milliequivalents of **4** per litre. For this titration, Zn(II) concentrations ranged from $2.5x10^{-7}$ to $2.7x10^{-3}$ M. LOD: 13 ppb.

*Using the hydrophilic film (**HP**)*

12 mm diameter discs were cut from **HP** and immersed for 12 hours in solutions with different Zn(II) concentrations (from $1x10^{-11}$ to $1x10^{-3}$ M) buffered at pH 4.66, to reach the complete equilibrium of the system. After that, discs were washed with the same buffer solution and measured in the fluorimeter. **Figure 4** shows the linear evolution of fluorescence intensity at 460 nm (excitation at 370 nm) when represented versus the logarithm of Zn(II) molarity, for concentrations ranging from $1x10^{-5}$ to $1x10^{-1}$ M and with error bars. The calculated limit of detection (LOD) of this system was 27 ppb.

On the other hand, the Job´s plot calculations confirm the observed stoichiometry with **WsP**, i.e., 1:1 (see **ESI**, **Section S5**, **Figure S7**). The complex formation constant between Zn(II) and **4** motifs was calculated from fitting the curve of fluorescence intensity versus Zn(II) concentration, yielding a value of $5.13x10^4$ (see **ESI**, **Section S6**, **Figure S9**). To carry out these calculations, an estimation of the number of **4** motifs inside each 12 mm diameter disc was necessary. This was calculated from ICP-MS results (see **ESI**, **Section S7**), and the resulting data was $2.97x10^{-7}$ mol/disc, which represents a molar ratio of 0.20%. This result was confirmed with an additional ICP-MS analysis for Zn(II) after saturation of all **4** motifs in **HP** (see **ESI**, **Table S4**).

Regarding response times, at high concentrations (100 mM) the response time of the sensory material was less than 10 min. However, the aim is to measure Zn(II) in biological media, where it can reach concentrations as high as 7-10 μM. Preliminary studies show that the response time with these concentrations could be around 4-5 hours. However, it is necessary to make even less concentrated points to build the calibration curve, and given the point of "proof of concept" of the research, the sensory discs were immersed overnight (12 hours) to make sure that the equilibrium was reached.

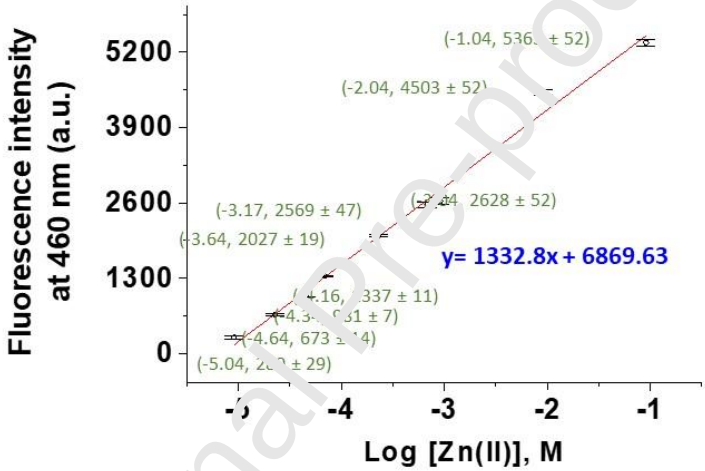

Figure 4. Titration of **HP** with Zn(II) in an aqueous solution buffered at pH 4.66. The 12 mm diameter discs were immersed in solutions with different Zn(II) concentrations (from $1x10^{-11}$ to $1x10^{-3}$ M). The graph shows the linear fitting of fluorescence intensity versus the logarithm of Zn(II) molarity between $1x10^{-5}$ and $1x10^{-1}$ M of Zn(II), with error bars. LOD: 27 ppb.

3.6. Determination of Zn(II) by the RGB method

12 mm diameter discs were cut from **HP** and immersed for 12 hours in solutions with different Zn(II) concentrations (from $1x10^{-7}$ to $1x10^{-1}$ M) buffered at pH 4.66, to reach the complete equilibrium of the system. After that, discs were washed with the same buffer solution and photographed in a retro-illumination lightbox for the extraction of RGB parameters. The graphical representation of the green component versus the logarithm of Zn(II) molarity results in a parabolic trend for concentrations ranging from $4.5x10^{-6}$ to $1x10^{-4}$ M, as displayed in **Figure 5**. We have taken into consideration only the green component because the red and blue components provide no relevant information.

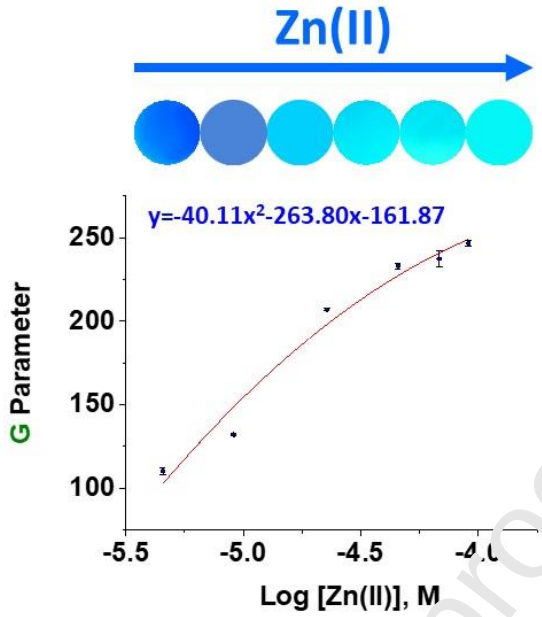

Figure 5. Graphical representation of the green component (G) of RGB parameters of the discs photographs versus the logarithm of Zn(II) molarity with error bars. Fitted curve for concentrations ranging from $4.5x10^{-6}$ to $1x10^{-4}$ M. RGB data can be found in **ESI**, **Section S8** and **Figure S10.**

3.7. pH study

A pH study was carried out with **HP** using the RGB method. A 12 mm diameter disc of **HP** was dipped in 250 ml of a 0.01 M Zn(II) solution. The pH of the solution was adjusted to 1 using HCl 0.1 M. The disc was photographed in the retro-illumination lightbox and pH was increased to 2 using NaOH 0.1 M. The procedure was repeated at 10 different pH values and, finally, the green parameter was graphically represented versus pH, as shown in **Figure 6**. The Zn(II):**4** complex is stable between pH 4 and pH 12, but very unstable at very acidic pHs. This behavior at pH below 3, allows the reusability of the material in a simple way, without using chelating reagents, by only dipping the films charged with Zn(II) in aqueous HCl.

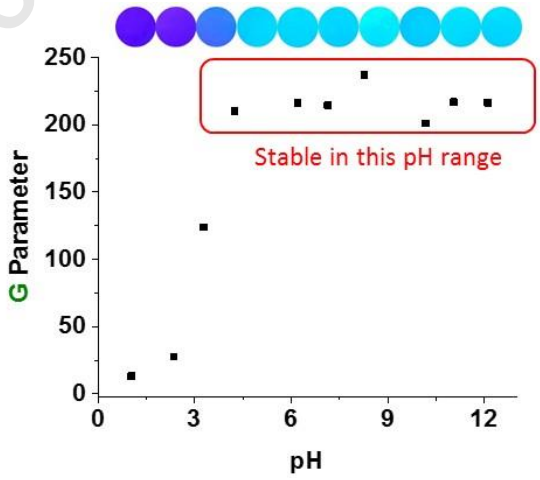

Figure 6. pH study carried out with the RGB method, by dipping a 12 mm diameter disc of **HP** in a 0.01 M Zn(II) solution and varying the pH. Graphical representation of the green parameter obtained from the photographs versus the pH of the solutions. RGB data can be found in **ESI**, **Section S9** and **Figure S11.**

3.8. Interference study

In this section we have considered several cations as possible interferents, regarding them as interferents if they can cause systematic errors (the definition of IUPAC is much centered on the magnitude of the systematic error caused in relation with the standard deviation of an unequivocally defined set of results) [44]. The study of possible interferents was performed in an aqueous solution buffered at pH 4.66, using 2 ml of a **WsP** solution (2.02 g/L, which corresponded to $4.52x10^{-2}$ milliequivalents of **4** per litre). The initial fluorescence of the solution was recorded in all cases. Then, 180 µl of an aqueous solution containing Zn(II) ($5x10^{-4}$ M) and interferent ($5x10^{-4}$ M) was added to the cuvette, and the fluorescence was recorded again. **Figure 7** shows the graphical representation of the normalized fluorescence intensity for all the measured interferents.

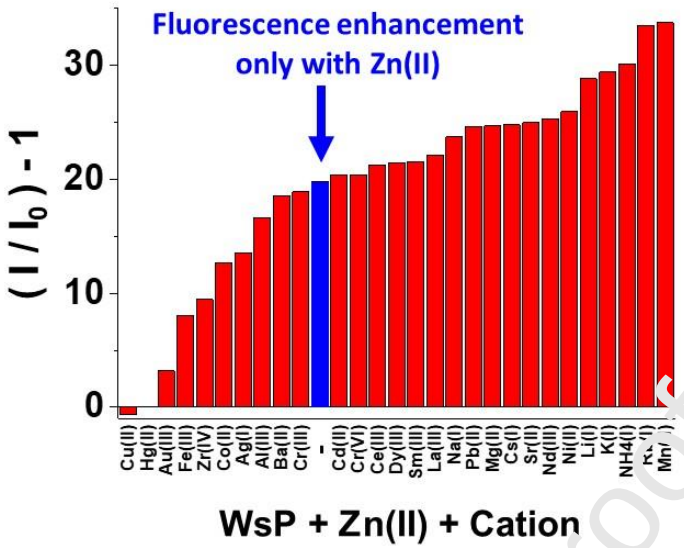

Figure 7. Interference study with 28 cations. Emission intensity enhancement (**(I/I₀)-1**) of a buffered aqueous solution of **WsP** (pH: 4.66, volume: 2 mL, concentration: 2.02 g/L, which corresponded to 4.52×10^{-2} milliequivalents of **4** per liter) after adding 180 µl of an aqueous solution containing Zn(II) (5×10^{-4} M) (blue bar), or Zn(II) (5×10^{-4} M) and interferent (5×10^{-4} M) (red bars). **I₀** is the emission intensity of the **WsP** buffered solution, and **I** the emission intensity after adding the cations.

As shown in **Figure 7**, cations as Cu(II) or Hg(II) are interferents of the detection system and switch off fluorescence. On the other hand, cations as Mn(II) or Rb(I) increase the fluorescence of the system significantly, so they are also interferents. However, they are not important interferents in the proposed real application of this sensor, i.e., the detection of Zn(II) in biological samples. In fact, our sensory material displays a behavior similar to that exhibited by 'Zinquin' (CAS number: 151606-29-0), a commercially available probe [30] that has been commonly used to detect zinc(II) in solution in biological media [31,32].

3.9. Proof of concept. Determination of Zn(II) in real biological samples

A real sample from chronic wounds was obtained from a human patient, following procedures established at Burgos University Hospital (HUBU) as described before. A swab was used to collect exudates from the chronic wounds, and then the swab was boiled for 10 minutes in a pH 4.66 buffer solution. The solution was filtered off, and each sample was measured fivefold with the reference method (ICP-MS). Additionally, a 12 mm diameter disc of **HP** was dipped in the solution for 24 hours. Finally, the disc was measured in a fluorimeter, and by the RGB method as previously depicted. The Zn(II) concentration in the solution was calculated from the calibration equations (sections 3.6 and 3.7), and the results are shown in **Figure 8**.

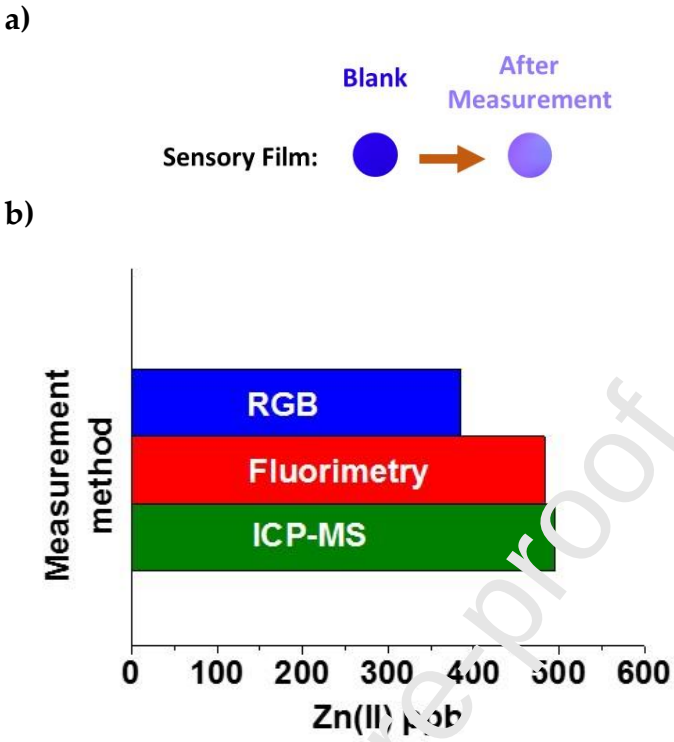

Figure 8. Results for the determination of Zn(II) in biological samples. **a)** Photos of an HA disc before and after dipping it in the biological solution. **b**) Zn(II) concentration data obtained from ICP-MS, fluorimetry and RGB method measurements.

As displayed in **Figure 8**, our material supposes a real alternative to the reference method (ICP-MS), both by using a fluorimeter and a smartphone to check the fluorescence change in the material. The results obtained using the proposed RGB method are relevant, even considering that the procedure is less accurate, because the overall procedure can be easily carried out by unskilled personnel, by using a smartphone to take a photo of the sensory material after dipping it in the exudate.

3.10. Comparative study of the sensor

Table 1 shows a study of the published detection methods for Zn(II), in terms of low-cost philosophy, naked-eye detection and the possibility of a hypothetical use in biological applications.

Table 1. Comparative table of different Zn(II) analytical methods.

Detection method	Low-cost	Biological applications	Naked-eye detection	Ref.
ICP-Mass & Laser Ablation	no	-	no	[45]
Fluorimetry-Probes in Solution	no	no	no	[48], [49], [51], [52]
	no	yes	no	[53], [46], [47], [50]
	no	yes	yes	[54], [55], [56], [57], [58], [59], [60], [61]
Fluorimetry -CHEF-type and ratiometric probes	no	yes	no	[62], [63]
Fluorimetry-Review	no	yes	no	[64]
Stopped-flow fluorescence study	no	yes	no	[65]
Potentiometric sensors	no	no	no	[66]
Electrochemical sensors	no	yes	no	[67]
Optical Fiber-Based UV-Vis spectrophotometry	no	no	no	[68]
Fluorimetry film-based sensor	no	yes	no	This work
Digital pictures (RGB parameters defining digital colors)	yes	yes	yes	This work

4. Conclusions

We have developed a new sensory method for the determination of Zn(II) in biological samples. The method is based on a polymeric material made of 99.75% of commercially available monomers. The material response can be measured by typical fluorimetry analysis, but also with our proposed RGB method. This method requires no reactants, no expensive equipment and the measurements can be easily carried out by unskilled personnel with a smartphone, by taking a picture of the material after dipping it in the exudate. This sensor works in a wide range of pH, and some characteristics of the material, such as response times or hydrophilicity, could be adapted "a la carte". The study, results, and conclusions presented here encourage us to deepen in the challenge of establishing a direct relationship between the Zn(II) concentration and the state/evolution of chronic wounds, a work that is now being carried out by our research team, involving many patients with to provide a reliable sensory material to be used as a simple and cheap method to follow the evolution of these wounds.

Conflicts of interest

There are no conflicts to declare.

Supplementary Materials

Synthesis and characterization of monomer and polymers, calculation of the stoichiometry of the Zn(II):**4** complex and complex formation constants of **WsP** and **HP** with Zn(II), RGB data, CIE 1931 xy chromaticity diagram, and X-ray crystallographic files in CIF format for **4** (CCDC 1992454) and Zn(II):**4** (CCDC 1992455).

Acknowledgements

We gratefully acknowledge the financial support provided by FEDER (Fondo Europeo de Desarrollo Regional), and both the Spanish Ministerio de Economía, Industria y Competitividad (MAT2017-84501-R) and the Consejería de Educación—Junta de Castilla y León (BU061U16) are gratefully acknowledged.

Data availability

The raw/processed data required to reproduce these findings cannot be shared at this time due to technical or time limitations. The data are available on request.

References

[1] V.J. Temple, A. Masta, Zinc in human health., P. N. G. Med. J. 47 (2004) 146–158. https://doi.org/10.9790/0853-13721823.

[2] R.A. Bozym, F. Chimienti, L.J. Giblin, G.W. Gross, O. Korichneva, Y. Li, S. Libert, W. Maret, M. Parviz, C.J. Frederickson, R.B. Thompson, Free zinc ions outside a narrow concentration range are toxic to a variety of cells in vitro, Exp. Biol. Med. 235 (2010) 741–750. https://doi.org/10.1258/ebm.2010.009250.

[3] C. Rica Mora Solera, M. Conte, A. Javier, R. Mora, H. Flores, D. Silva, Papel de las Metaloproteinasas de la Matriz en la Degradación del Tejido Pulpar: Una revisión literaria, Rev. Científica Odontológica. 1 (2005) 20–26. www.merops.ac.uk (accessed April 28, 2020).

[4] A. Tezvergil-Mutluay, K.A. Agee, T. Hoshika, M. Carrilho, L. Breschi, L. Tjäderhane, Y. Nishitani, R.M. Carvalho, S. Looney, F.R. Tay, D.H. Pashley, The requirement of zinc and calcium ions for functional MMP activity in demineralized dentin matrices, Dent. Mater. 26 (2010) 1059–1067. https://doi.org/10.1016/j.dental.2010.07.006.

[5] C.D. Tran, R. Katsikeros, N. Manton, N.F. Krebs, K.M. Hambidge, R.N. Butler, G.P. Davidson, Zinc homeostasis and gut function in children with celiac disease, Am. J. Clin. Nutr. 94 (2011) 1026–1032. https://doi.org/10.3945/ajcn.111.018093.

[6] S.S. Martinez, A. Campa, Y. Li, C. Fleetwood, T. Stewart, V. Ramamoorthy, M.K. Baum, Low Plasma Zinc Is Associated with Higher Mitochondrial Oxidative Stress and Faster Liver Fibrosis Development in the Miami Adult Studies in HIV Cohort, J. Nutr. 147 (2017) 556–562. https://doi.org/10.3945/jn.116.243832.

[7] J. Mohammed, S. Mehrotra, H. Schulz, R. Lim, Severe Infant Rash Resistant to Therapy Due to Zinc Deficiency, Pediatr. Emerg. Care. 33 (2017) 582–584. https://doi.org/10.1097/PEC.0000000000001218.

[8] I. Rotter, D.I. Kosik-Bogacka, B. Dołęgowska, K. Safranow, M. Kuczyńska, M. Laszczyńska, Analysis of the relationship between the blood concentration of several metals, macro- and micronutrients and endocrine disorders associated with male aging, Environ. Geochem. Health.

38 (2016) 749–761. https://doi.org/10.1007/s10653-015-9758-0.

[9] P. Zorrilla, L.A. Gómez, J.A. Salido, A. Silva, A. López-Alonso, Low serum zinc level as a predictive factor of delayed wound healing in total hip replacement, Wound Repair Regen. 14 (2006) 119–122. https://doi.org/10.1111/j.1743-6109.2006.00100.x.

[10] P.H. Lin, M. Sermersheim, H. Li, P.H.U. Lee, S.M. Steinberg, J. Ma, Zinc in wound healing modulation, Nutrients. 10 (2018) 16. https://doi.org/10.3390/nu10010016.

[11] S. Kogan, A. Sood, M.S. Garnick, Zinc and Wound Healing: A Review of Zinc Physiology and Clinical Applications, Wounds a Compend. Clin. Res. Pract. 29 (2017) 102–106. https://doi.org/102-106 PMID: 28448263.

[12] A.B.G. Lansdown, U. Mirastschijski, N. Stubbs, E. Scanlon, M.S. Ågren, Zinc in wound healing: Theoretical, experimental, and clinical aspects, Wound Repair Regen. 15 (2007) 2–16. https://doi.org/10.1111/j.1524-475X.2006.00179.x.

[13] S.K. Ghosh, P. Kim, X.A. Zhang, S.H. Yun, A. Moore, S.J. Lippard, Z. Medarova, A novel imaging approach for early detection of prostate cancer based on endogenous zinc sensing, Cancer Res. 70 (2010) 6119–6127. https://doi.org/10.1158/0008-5472.CAN-10-1008.

[14] R.M. Atwater, The Merck Manual of Diagnosis and Therapy, Merck Sharpe & Dohme Research Laboratories, 1950. https://doi.org/10.2105/ajph.40.11.1454.

[15] K. T, T. I, H. R, Y. H, I. M, Y. Y, N. K, Selenium, zinc, copper and cadmium concentration in livers and kidneys of people exposed to environmental cadmium., J. Trace Elem. Electrolytes Health Dis. 2 (1988) 101–104.

[16] R. Cornelis, F. Borguet, J. De Kimpe, Trace elements in medicine. Speciation: the new frontier, Anal. Chim. Acta. 283 (1993) 183–192. https://doi.org/10.1016/0003-2670(93)85221-5.

[17] N. Fabris, E. Mocchegiani, Zinc, human diseases and aging, Aging Clin. Exp. Res. 7 (1995) 77–93. https://doi.org/10.1007/BF03324297.

[18] S. Chan, B. Gerson, S. Subramaniam, The role of copper, molybdenum, selenium, and zinc in nutrition and health, Clin. Lab. Med. 18 (1998) 673–685. https://doi.org/10.1016/s0272-2712(18)30143-4.

[19] K.P. Carter, A.M. Young, A.E. Palmer, Fluorescent sensors for measuring metal ions in living systems, Chem. Rev. 114 (2014) 4564–4601. https://doi.org/10.1021/cr400546e.

[20] B. Wang, Y. Hu, Z. Su, Synthesis and photophysical behaviors of a blue fluorescent copolymer as chemosensor for protons and Ni2+ ion in aqueous solution, React. Funct. Polym. 68 (2008) 1137–1143. https://doi.org/10.1016/j.reactfunctpolym.2008.03.005.

[21] D. Zeng, J. Cheng, S. Ren, J. Sun, H. Zhong, E. Xu, J. Du, Q. Fang, A new sensor for copper(II) ion based on carboxyl acid groups substituted polyfluoreneethynylene, React. Funct. Polym. 68 (2008) 1715–1721. https://doi.org/10.1016/j.reactfunctpolym.2008.10.001.

[22] J.L. Pablos, S. Ibeas, A. Muñoz, F. Serna, F.C. García, J.M. García, Solid polymer and metallogel networks based on a fluorene derivative as fluorescent and colourimetric chemosensors for Hg(II), React. Funct. Polym. 79 (2014) 14–23. https://doi.org/10.1016/j.reactfunctpolym.2014.02.009.

[23] R.S. Juang, P.C. Yang, H.W. Wen, C.Y. Lin, S.C. Lee, T.W. Chang, Synthesis and chemosensory properties of terpyridine-containing diblock polycarbazole through RAFT polymerization, React. Funct. Polym. 93 (2015) 130–137. https://doi.org/10.1016/j.reactfunctpolym.2015.06.008.

[24] A.M. Sanjuán, J.A. Reglero Ruiz, F.C. García, J.M. García, Recent developments in sensing devices based on polymeric systems, React. Funct. Polym. 133 (2018) 103–125. https://doi.org/10.1016/j.reactfunctpolym.2018.10.007.

[25] J.A.R. Ruiz, A.M. Sanjuán, S. Vallejos, F.C. García, J.M. García, Smart polymers in micro and nano sensory devices, Chemosensors. 6 (2018) 12. https://doi.org/10.3390/chemosensors6020012.

[26] K. Boonkitpatarakul, A. Smata, K. Kongnukool, S. Srisurichan, K. Chainok, M. Sukwattanasinitt, An 8-aminoquinoline derivative as a molecular platform for fluorescent sensors for Zn(II) and Cd(II) ions, J. Lumin. 198 (2018) 59–67. https://doi.org/10.1016/j.jlumin.2018.01.048.

[27] C.J. Fahrni, T. V. O'Halloran, Aqueous coordination chemistry of quinoline-based fluorescence probes for the biological chemistry of zinc, J. Am. Chem. Soc. 121 (1999) 11448–11458. https://doi.org/10.1021/ja992709f.

[28] M.R. Karim, D.H. Petering, Newport Green, a fluorescent sensor of weakly bound cellular Zn2+: Competition with proteome for Zn2+, Metallomics. 8 (2016) 201–210. https://doi.org/10.1039/c5mt00167f.

[29] S. Mukherjee, S. Talukder, A reversible luminescent quinoline based chemosensor for recognition of Zn2+ ions in aqueous methanol medium and its logic gate behavior, J. Lumin. 177 (2016) 40–47. https://doi.org/10.1016/j.jlumin.2016.04.016.

[30] Zinquin, ≥95% (HPLC), solid | C19H18N2O5S | Sigma-Aldrich, (n.d.). https://www.sigmaaldrich.com/catalog/product/sial/z2376?lang=es&region=ES (accessed April 28, 2020).

[31] P.D. Zalewski, I.J. Forbes, W.H. Betts, Correlation of apoptosis with change in intracellular labile Zn(II) using Zinquin [(2-methyl-8-p-toluenesulphonamido-6-quinolyloxy)acetic acid], a new specific fluorescent probe for Zn(II), Biochem. J. 296 (1993) 403–408. https://doi.org/10.1042/bj2960403.

[32] C.D. Geddes (editor), Reviews in Fluorescence 2004, Springer, 2004. https://doi.org/10.1007/978-0-306-48672-2.

[33] S. Vallejos, A. Muñoz, S. Ibeas, F. Serna, F.C. García, J.M. García, Solid sensory polymer substrates for the quantification of iron in blood, wine and water by a scalable RGB technique, J. Mater. Chem. A. 1 (2013) 15435–15441. https://doi.org/10.1039/c3ta12703f.

[34] S. Vallejos, J.A. Reglero, F.C. García, J.M. García, Direct visual detection and quantification of mercury in fresh fish meat using facilely prepared polymeric sensory labels, J. Mater. Chem. A. 5 (2017) 13710–13716. https://doi.org/10.1039/c7ta03902f.

[35] S. Vallejos, A. Muñoz, S. Ibeas, F. Serna, F.C. García, J.M. García, Forced solid-state interactions for the selective Turn-On fluorescence sensing of aluminum ions in water using a sensory polymer substrate, ACS Appl. Mater. Interfaces. 7 (2015) 921–928. https://doi.org/10.1021/am507458k.

[36] A.M. Brouwer, Standards for photoluminescence quantum yield measurements in solution

(IUPAC technical report), Pure Appl. Chem. 83 (2011) 2213–2228. https://doi.org/10.1351/PAC-REP-10-09-31.

[37] M. Guembe-García, P.D. Peredo-Guzmán, V. Santaolalla-García, N. Moradillo-Renuncio, S. Ibeas, A. Mendía, F.C. García, J.M. García, S. Vallejos, Why the sensory response of organic probes is different in solution and in the solid- state within a polymer film? Evidence and application to the detection of amino acids in human chronic wounds Marta Guembe-García, Unpubl. Work. (n.d.).

[38] L.O.I.I. Cie, P. Cie, Commission Internationale De L ' Éclairage International Commission on Illumination Internationale Beleuchtungskomm, 1931 (1993). http://files.cie.co.at/204.xls (accessed April 28, 2020).

[39] M.K. Chun, J. Cho, A.R. Jeong, K.S. Min, J.H. Jeong, Tetrahedral Zinc(II) Complexes with Chiral Diamine Ligands: Synthesis, Characterization, and Photoluminescence, Bull. Korean Chem. Soc. 40 (2019) 921–924. https://doi.org/10.1002/bkcs.11845.

[40] A. Ayadi, M.A. Benmensour, Y. Cheret, A. Boucekkine, A. El-Ghayoury, Zinc and copper complexes of stilbene iminopyridine ligands with η2-Olefin binding mode, J. Organomet. Chem. 858 (2018) 14–22. https://doi.org/10.1016/j.jorganchem.2018.01.002.

[41] T.M. Chang, S. Sinharay, A. V. Astashkin, E. Tomat, Prodigiosin analogue designed for metal coordination: Stable zinc and copper pyrrolyldipyrrins, Inorg. Chem. 53 (2014) 7518–7526. https://doi.org/10.1021/ic5008439.

[42] M.J. Minch, An Introduction to Hydrogen Bonding (Jeffrey, George A.), Oxford University Press, 1999. https://doi.org/10.1021/ed076p1591.

[43] T. Steiner, The hydrogen bond in the solid state, Angew. Chemie - Int. Ed. 41 (2002) 48–76. https://doi.org/10.1002/1521-3773(20020104)41:1<48::AID-ANIE48>3.0.CO;2-U.

[44] J. Bartos, M.P. Roussel-Uclaf, International union of pure and applied chemistry analytical chemistry division commission on analytical reactions and reagents spectrophotometric and fluorimetric determination of amines, Pure Appl. Chem. 56 (1984) 467–477. https://doi.org/10.1351/pac198456040467.

[45] P. Arrowsmith, Laser Ablation of Solids for Elemental Analysis by Inductively Coupled Plasma Mass Spectrometry, 1987. https://doi.org/10.1021/ac00137a014.

[46] M. Ui, Y. Tanaka, Y. Araki, T. Wada, T. Takei, K. Tsumoto, S. Endo, K. Kinbara, Application of photoactive yellow protein as a photoresponsive module for controlling hemolytic activity of staphylococcal α-hemolysin, Chem. Commun. 48 (2012) 4764–4766. https://doi.org/10.1039/c2cc30963g.

[47] Y. Ding, Y. Xie, X. Li, J.P. Hill, W. Zhang, W. Zhu, Selective and sensitive "turn-on" fluorescent Zn2+ sensors based on di- and tripyrrins with readily modulated emission wavelengths, Chem. Commun. 47 (2011) 5431–5433. https://doi.org/10.1039/c1cc11493j.

[48] F. Wang, R. Peng, Y. Sha, Selective dendritic fluorescent sensors for Zn(II), Molecules. 13 (2008) 922–930. https://doi.org/10.3390/molecules13040922.

[49] Z. Wu, Q. Chen, G. Yang, C. Xiao, J. Liu, S. Yang, J.S. Ma, Novel fluorescent sensor for Zn(II) based on bis(pyrrol-2-yl- methyleneamine) ligands, Sensors Actuators, B Chem. 99 (2004) 511–515. https://doi.org/10.1016/j.snb.2003.12.070.

[50] S. Erdemir, S. Malkondu, Calix[4]arene based a NIR-fluorescent sensor with an enhanced stokes shift for the real-time visualization of Zn(II) in living cells, Sensors Actuators, B Chem. 306 (2020) 127574. https://doi.org/10.1016/j.snb.2019.127574.

[51] G. Ambrosi, M. Micheloni, D. Paderni, M. Formica, L. Giorgi, V. Fusi, Fluorescent macrocyclic chemosensor for Zn(II) detection at alkaline pH values, Supramol. Chem. 32 (2020) 139–149. https://doi.org/10.1080/10610278.2020.1713324.

[52] E. Tamanini, K. Flavin, M. Motevalli, S. Piperno, L.A. Gheber, M.H. Todd, M. Watkinson, Cyclam-based "clickates": Homogeneous and heterogeneous fluorescent sensors for Zn(II), Inorg. Chem. 49 (2010) 3789–3800. https://doi.org/10.1021/ic901939x.

[53] M. Hagimori, M. Taniura, N. Mizuyama, Y. Karimine, S. Kawakami, H. Saji, T. Mukai, Synthesis of a novel pyrazine-pyridone biheteroaryl-based fluorescence sensor and detection of endogenous labile zinc ions in lung cancer cells, Sensors (Switzerland). 19 (2019) 2049. https://doi.org/10.3390/s19092049.

[54] Y. Upadhyay, T. Anand, L.T. Babu, P. Paira, G. Crisponi, A.K. Sk, P. Kumar, S.K. Sahoo, Three-in-one type fluorescent sensor based on a pyrene pyridoxal cascade for the selective detection of Zn(II), hydrogen phosphate and cysteine, Dalt. Trans. 47 (2018) 742–749. https://doi.org/10.1039/c7dt04234e.

[55] T. Anand, A.S.K. Kumar, S.K. Sahoo, A novel Schiff base derivative of pyridoxal for the optical sensing of Zn2+ and cysteine, Photochem. Photobiol. Sci. 17 (2018) 414–422. https://doi.org/10.1039/c7pp00391a.

[56] T. Anand, A. Kumar SK, S.K. Sahoo, Vitamin B_6 Cofactor Derivative: A Dual Fluorescent Turn-On Sensor to Detect Zn^{2+} and CN^- Ions and Its Application in Live Cell Imaging, ChemistrySelect. 2 (2017) 7570–7579. https://doi.org/10.1002/slct.201701024.

[57] K. Tayade, S.K. Sahoo, B. Bondhopadhyay, V.K. Bhardwaj, N. Singh, A. Basu, R. Bendre, A. Kuwar, Highly selective turn-on fluorescent sensor for nanomolar detection of biologically important Zn2+ based on isonicotinohydrazide derivative: APPLICATION in cellular imaging, Biosens. Bioelectron. 61 (2014) 429–433. https://doi.org/10.1016/j.bios.2014.05.053.

[58] U.A. Fegade, S.K. Sahoo, A. Singh, N. Singh, S.B. Attarde, A.S. Kuwar, A chemosensor showing discriminating fluorescent response for highly selective and nanomolar detection of Cu2+ and Zn2+ and its application in molecular logic gate, Anal. Chim. Acta. 872 (2015) 63–69. https://doi.org/10.1016/j.aca.2015.02.051.

[59] R. Selva Kumar, S.K. Ashok Kumar, K. Vijayakrishna, A. Sivaramakrishna, P. Paira, C.V.S. Brahmmananada Rao, N. Sivaraman, S.K. Sahoo, Bipyridine bisphosphonate-based fluorescent optical sensor and optode for selective detection of Zn2+ ions and its applications, New J. Chem. 42 (2018) 8494–8502. https://doi.org/10.1039/c8nj00158h.

[60] K. Tayade, B. Bondhopadhyay, K. Keshav, S.K. Sahoo, A. Basu, J. Singh, N. Singh, D.T. Nehete, A. Kuwar, A novel zinc(II) and hydrogen sulphate selective fluorescent "turn-on" chemosensor based on isonicotiamide: INHIBIT type's logic gate and application in cancer cell imaging, Analyst. 141 (2016) 1814–1821. https://doi.org/10.1039/c5an02295a.

[61] N. Khairnar, K. Tayade, S.K. Sahoo, B. Bondhopadhyay, A. Basu, J. Singh, N. Singh, V. Gite, A. Kuwar, A highly selective fluorescent "turn-on" chemosensor for Zn2+ based on a benzothiazole

conjugate: Their applicability in live cell imaging and use of the resultant complex as a secondary sensor of CN-, Dalt. Trans. 44 (2015) 2097–2102. https://doi.org/10.1039/c4dt03247k.

[62] N.C. Lim, J. V. Schuster, M.C. Porto, M.A. Tanudra, L. Yao, H.C. Freake, C. Brückner, Coumarin-based chemosensors for zinc(II): Toward the determination of the design algorithm for CHEF-type and ratiometric probes, Inorg. Chem. 44 (2005) 2018–2030. https://doi.org/10.1021/ic048905r.

[63] Y. Lv, M. Cao, J. Li, J. Wang, A sensitive ratiometric fluorescent sensor for zinc(II) with high selectivity, Sensors (Switzerland). 13 (2013) 3131–3141. https://doi.org/10.3390/s130303131.

[64] R. Pandey, A. Kumar, Q. Xu, D.S. Pandey, Zinc(ii), copper(ii) and cadmium(ii) complexes as fluorescent chemosensors for cations, Dalt. Trans. 49 (2020) 542–568. https://doi.org/10.1039/c9dt03017d.

[65] E.M. Nolan, S.J. Lippard, Small-molecule fluorescent sensors for investigating zinc metalloneurochemistry, Acc. Chem. Res. 42 (2009) 193–203. https://doi.org/10.1021/ar8001409.

[66] M.A. Abbasi, Z.H. Ibupoto, M. Hussain, Y. Khan, A. Khan, O. Nur, M. Willander, Potentiometric zinc ion sensor based on honeycomb-Like NiO nanostructures, Sensors (Switzerland). 12 (2012) 15424–15437. https://doi.org/10.3390/s121115424.

[67] J. Kudr, H.V. Nguyen, J. Gumulec, L. Nejdl, I. Blazkova, B. Ruttkay-Nedecky, D. Hynek, J. Kynicky, V. Adam, R. Kizek, Simultaneous automatic electrochemical detection of zinc, cadmium, copper and lead ions in environmental samples using a thin film mercury electrode and an artificial neural network, Sensors (Switzerland). 15 (2014) 592–610. https://doi.org/10.3390/s150100592.

[68] S. Kopitzke, P. Geissinger, An optical fiber based sensor array for the monitoring of zinc and copper ions in aqueous environments, Sensors (Switzerland). 14 (2014) 3077–3094. https://doi.org/10.3390/s140203077.

CRediT author statement

Marta Guembe-García: formal analysis, investigation, resources, writing – original draft; writing – original draft. **Saúl Vallejos:** Conceptualization, investigation, methodology, supervision, writing – original draft, writing – review & editing. **Israel Carreira-Barral:** investigation, resources. **Saturnino Ibeas:** formal analysis, methodology. **Félix C. García:** Conceptualization, methodology, project administration, supervision, writing – review & editing. **Victoria Santaolalla-García:** Conceptualization, investigation, resources, writing – original draft. **Natalia Moradillo-Renuncio:** Conceptualization, investigation, resources, , writing – original draft. **José M. García:** Conceptualization, funding acquisition, methodology, project administration, supervision, writing – review & editing.

Declaration of interests

☒ The authors declare that they have no known competing financial interests or personal relationships that could have appeared to influence the work reported in this paper.

☐The authors declare the following financial interests/personal relationships which may be considered as potential competing interests:

Highlights

- Sensory materials increase their fluorescence in presence of zinc (II) in biological media
- The sensory materials are polymers with chemically anchored sensory motifs
- The sensory materials are films shaped crosslinked polymers and also water-soluble polymers
- As a proof of concept, the Zn(II) content of a human chronic wound was estimated